Harnessing the Polariton Drag Effect to Design an Electrically Controlled Optical Switch

Oleg L. Berman, Roman Ya. Kezerashvili, and German V. Kolmakov*

Physics Department, New York City College of Technology, City University of New York, Brooklyn, New York 11201, United States

ABSTRACT We propose a design of a Y-shaped electrically controlled optical switch based on the studies of propagation of an exciton–polariton condensate in a patterned optical microcavity with an embedded quantum well. The polaritons are driven by a time-independent force due to the microcavity wedge shape and by a time-dependent drag force owing to the interaction of excitons in a quantum well and the electric current running in a neighboring quantum well. It is demonstrated that by applying the drag force one can direct more than 90% of the polariton flow toward the desired branch of the switch with no hysteresis. By considering the transient dynamics of the polariton condensate, we estimate the response speed of the switch as 9.1 GHz. We also propose a design of the polariton switch in a flat microcavity based on the geometrically identical Y-shaped quantum wells where the polariton flow is only induced by the drag force. The latter setup enables one to design a multiway switch that can act as an electrically controlled optical transistor with on and off functions. Finally, we performed the simulations for a microcavity with an embedded gapped graphene layer and demonstrated that in this case the response speed of the switch can be increased up to 14 GHz for the same switch size. The simulations also show that the energy gap in the quasiparticle spectrum in graphene can be utilized as an additional parameter that controls the propagation of the signals in the switch.

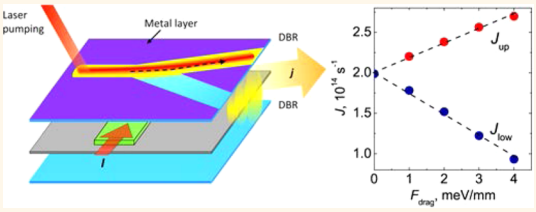

KEYWORDS: optical circuits · nanostructures · exciton polaritons · drag force · graphene

In the past decades, substantial experimental and theoretical efforts were devoted to find the optimal ways to tune the optical properties of semiconductors and graphene by application of external electric and magnetic fields. The motivation of the research in this field lies in the potential applications for integrated circuits in optical and quantum computers, for secure information transfer, and in new light sources.[1] One of the promising approaches is in the use of polaritons, which are a quantum superposition of cavity photons and excitons in a nanometer-wide semiconductor layer (a quantum well).[2−5] Since polaritons are interacting Bose particles, a polariton gas can transit to a superfluid state that, under certain conditions, propagates in a microcavity almost without dissipation.[6−9] Because of a small effective mass, 10^{-4} of the free electron mass, the superfluid transition occurs at relatively high temperatures that are comparable with the room temperature. Polaritons can propagate in the sample with a speed up to a few percent of the speed of light, which is much faster than that of electric-field driven electrons and holes in semiconductors.[10] However, one of the main problems to be solved in actual design of polariton-based optical devices is in weak response of polaritons to an external electric field owing to their net zero electric charge.

In this paper, we propose a design of polariton-based, electrically controlled switch, in which the polariton propagation is controlled by means of a drag force. Recently, it was shown that the drag caused by an electric current results in entrainment of polaritons and in formation of a persistent, directed polariton current in the microcavity.[11,12] The force is exerted on the exciton component of polaritons.[13] The drag results in generation of the polariton flux proportional to the driving electric field **E**,

$$\mathbf{j} = \gamma \mathbf{E} \qquad (1)$$

where γ is the temperature-dependent drag coefficient. In addition to the electrically controlled drag force, the polaritons can also

* Address correspondence to gkolmakov@citytech.cuny.edu.

Received for review July 10, 2014 and accepted September 29, 2014.

Published online September 29, 2014
10.1021/nn503787q

be accelerated by a constant, time independent force, which is caused by the wedge-like shape of the microcavity.[14,15]

In this paper, we propose the polariton switches of two types. In the first design, the polariton flow in the switch is produced by a constant force due to the wedge-like shape of the microcavity whereas the drag force is utilized to switch the direction of the flow. In the second design, the polariton flow in the required direction is only produced by the drag force. In both cases, the photons propagate in the microcavity, and the excitons are located in a quantum well (QW) embedded in the microcavity. Below we describe the both types of the switches in details.

In the first design, we take advantage of a patterned microcavity to create a potential-energy landscape for polaritons in the form of one-dimensional channels, or "polariton wires", which are somewhat similar to the ordinary wires that conduct electrical current. However, in our case, the wires conduct polaritons and help one to transport photons to a desired location in the semiconductor structure. Recently developed experimental techniques, which enable one to produce such guiding potentials for polaritons, include deposition of a metal pattern on the Bragg reflectors,[16] modulation of the cavity layer thickness in a mesa structure,[17,18] or varying the chemical composition of the structure during epitaxial growth.[19] The polariton channels of complex shape and topology can also be engineered directly in an air-filled microcavity by creating quasi-one-dimensional waveguides, or micropillars.[20−23]

To design a polariton switch, we utilize a Y-shaped channel shown in Figure 1. We assume that polaritons are created at a constant rate by the external laser pumping at the stem of the channel, and then propagate toward the junction under the action of a constant force due to the microcavity wedge-like shape. After reaching the junction, the polariton flow splits between the two branches. If no drag force is applied to the polaritons, the flux is distributed equally between the branches. However, if the drag force is exerted on the polaritons in the region of the junction in the direction normal to the stem, the polaritons are "pushed" toward one branch and hence, the flux in that branch increases. Simultaneously, the flux through another branch decreases due to approximate conservation of the total number of polaritons and in effect, the polariton flux is redistributed between the branches. The drag force in the junction region is produced by the electric current running in a neighboring quantum well, which has a form of a stripe placed in a microcavity perpendicular to the stem of the channel. Thus, the heterostructure encompasses two parallel quantum wells, separated by a nanometer-wide semiconductor or dielectric barrier, placed in an optical microcavity. We demonstrate below that more than 90% of the total polariton flux can be dynamically redistributed between the branches for realistically achievable drag forces.

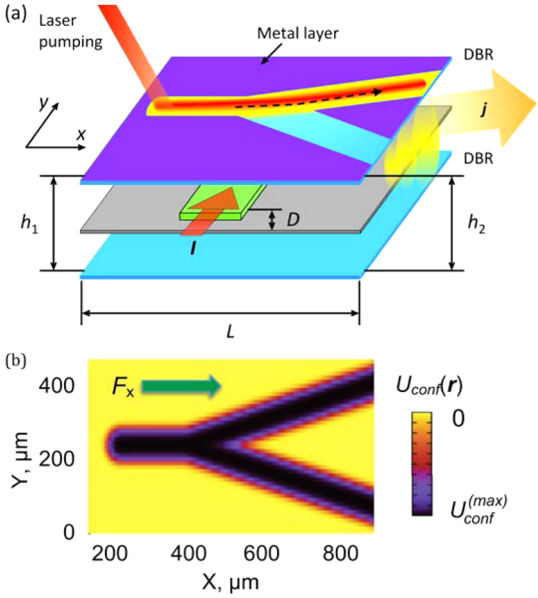

Figure 1. (a) Schematic of the wedge-shaped microcavity formed by two distributed Bragg reflectors (DBR) that encompasses an embedded quantum well. The excitons are located in a quantum well (gray) between the reflectors. Polaritons in the microcavity are formed as a quantum superposition of excitons and cavity photons. The force F_x is exerted on the polaritons in x-direction owing to a small opening angle $\alpha \approx (h_2 - h_1)/L \ll 1$ of the microcavity, where h_1 and h_2 are the microcavity lengths at the opposite edges and L is the horizontal size of the microcavity. A metal layer deposited on the upper DBR creates a Y-shaped potential energy landscape for the polaritons shown in Figure (b). The maximum depth of the channel formed by the energy landscape, $U_{conf}^{(max)}$, is defined in the text. The polaritons are created by an external laser radiation in the stem of the channel and propagate toward the junction due to the force F_x. A driving electric current I runs perpendicularly to the stem of the channel in a quantum well (green) located at the junction at a distance D from the quantum well with the excitons. The polariton flux j propagates along one branch of the channel in response to the drag created by the current. The polariton switch is also considered for the case where the quantum well is changed to a gapped graphene layer.

The second type of the polariton switch is based on a flat microcavity where the mirrors are parallel to each other. In this design, the excitons are located in a Y-shaped semiconductor quantum well, see Figure 2. The neighboring current-carrying quantum well is geometrically identical to this structure. In contrast to the switch of the first type described above, in this design we do not use the patterned microcavity. Instead, the polaritons are guided by the Y-shaped structure. The electric current in the quantum well is generated by the external voltage. The drag force exerted on the cavity polaritons by the electric current is directed parallel to the channel and induces the polariton flow along one of the branches. The polariton flow is redistributed between the branches in response to switching electric voltage applied to the current-carrying quantum well.

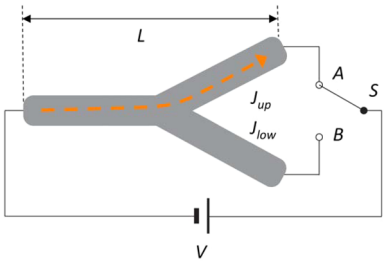

Figure 2. Schematic of the polariton switch where the polariton flux in a flat microcavity is induced by the drag due to an electric current running in the circuit. Both the current-carrying quantum well and the quantum well containing the excitons have identical geometrical Y shape and are positioned parallel to each other. The diffraction Bragg reflectors are positioned parallel to the quantum wells and the quantum well and are not shown. The position of switch *S* controls the direction of the polariton flow.

The advantage of this design is 2-fold. First, it enables one to reverse the polarity of the driving voltage and, in effect, to apply the drag force that "pushes" the polaritons toward the excitation spot. In this case, the polariton flow in the channel is not formed. Thus, this design allows one to realize a *three-way switch* that enables one not only to redistribute the photons between the branches but also to block the photon propagation. The proposed design can be used as an electrically controlled optical transistor, which can block the photon propagation in response to the external signals. Second, this design can also potentially be extended to more complicated topology with three and more output channels to create a *multistate* optical switch.

Optical transistors are now under active consideration, including those controlled by electric or optical signals.[24−27] Recently, an electrically controlled diode has been designed based on the optical bistability in a GaAs-based microcavity.[28] In that setup, the regimes of weak and strong exciton-photon coupling were reversibly switched by applying an external, controlling electric field. The off-to-on ratio of the transmitted signal of the diode varied from 1/5 to 1/10 depending on the bias voltage,[28] which is close to that in our design. Similar off-to-on ratio in the signal was demonstrated for all-optical transistors.[26] However, in contrast to the electrically controlled diode,[28] our design does not show the hysteresis between the states and thus, it is suited as a switching element in integrated circuits. Specifically, the electrically controlled optical switch can be utilized a routing element that conjunct the optical circuits with the peripheral electronics.

The energy consumption of a device is a parameter important for its practical use in integrated circuits. One can estimate the Joule heat released on the proposed device under relevant experimental conditions. The experiments relevant to the electron−hole Coulomb drag effect have been performed for GaAs/AlGaAs quantum wells.[29,30] In these measurements, the simple bar mesas were fabricated with the width $w = 40\ \mu$m and length $l = 400\ \mu$m; the thickness of the quantum wells was 20 nm;[29] the separation between quantum wells in the samples was $D = 20$ or 30 nm.[30] The applied dc driving current was less than $I = 1$ nA.[30] The heat P released per unit time from GaAs/AlGaAs coupled quantum wells due to Coulomb drag is estimated as $P = I(V_{drag} + V_{xx})$, where $V_{drag} = I\rho_{drag}l/w$ is the drag voltage across the quantum well with the dragged quasiparticles, ρ_{drag} is the drag resistivity,[29] $V_{xx} = I\rho_{xx}l/w$ is the voltage across the quantum well that carries the driving current, and ρ_{xx} is the resistivity of GaAs quantum well. At $T = 3$ K and the carrier density $n_{car} = 6 \times 10^{14}$ m^{-2} the measurements gave $\rho_{xx} = 0.1\ \Omega$ and $\rho_{drag} = 0.5\ \Omega$.[30,31] Thus, the estimate of the heat released per unit time from GaAs/AlGaAs coupled quantum wells due to Coulomb drag gives $P = 6 \times 10^{-18}$ W, which is much lower than $P \sim 10^{-8}$ W per transistor in modern computer microchips.

In our design, the quantum wells containing the excitons can be fabricated by using a number of materials, including GaAs,[32,33] CdTe,[34] WSe_2,[35] and gapped graphene.[36,37] In this paper, we focus on GaAs quantum wells since this material is widely used in the practical design and fabrication of optical cavities.[38,39] We also performed the simulations for a microcavity with an embedded gapped graphene layer and compare the results with those for a microcavity with an embedded GaAs quantum well. Superfluidity of an exciton−polariton condensate has recently been considered for microcavities with embedded gapped graphene.[9] The advantage of gapped graphene is in the possibility of tuning the mass and the sound velocity in the spectrum of quasiparticles by changing the energy gap between the valence and conduction bands[40] and through that to optimize the performance of the system. The energy gap in graphene can be created and changed in a wide range by applying the external electric field.[41−43] Another advantage of considering excitons in a graphene layer is in the absence of the fluctuations of the width due to the fact that graphene is a two-dimensional one atomically thin layer. Thus, the use of graphene can help to avoid difficulties related to scattering of the polaritons on structural defects in the microcavities. Additionally, the drag in graphene dominates in a wide range of temperatures.[44]

RESULTS AND DISCUSSION

Electrically Controlled Optical Switch in a Wedge-Shaped Microcavity. We study propagation of the polariton condensate in a patterned microcavity by numerically integrating the nonequilibrium Gross−Pitaevskii equation for the wave function $\Psi(\mathbf{r}, t)$ of the polariton condensate in the microcavity. (Here, $\mathbf{r} = (x, y)$ is a two-dimensional vector in the plane of the microcavity, and t is time.) The model is described in detail in the Methodology section. Specifically, we determine

the conditions that enable one to control the polariton spreading in a potential landscape.

The layered semiconductor structure considered in this section is shown in Figure 1a. The excitons are positioned in the quantum well embedded in the microcavity. The free electrons are located in the neighboring, parallel quantum well that has a form of a stripe and placed at the junction of the Y-shaped channel perpendicularly to the channel stem. In the simulations, we used the value of the drag coefficient γ corresponding to the distance between the quantum well and the stripe equal $D = 17.5$ nm.[11] The decrease of the distance D results in rising drag and thus in stronger entrainment of the polariton quasiparticles by the driving electric current. The heterostructure is placed between two high-quality multilayer mirrors (distributed Bragg reflectors, or DBR). Figure 1b demonstrates the Y-shaped potential-energy landscape for the polaritons due to patterning of the microcavity. The reflectors form a wedge opened toward the positive direction of the x-axis (that is, to the right in Figure 1) that results in a constant force exerted on the polaritons in a microcavity, as explained in Methodology. In the simulation, we vary the constant force F_x in the range from 0.5 to 19 meV/mm that corresponds to the representative experimental values.[14,15] The polaritons are created by an external laser radiation in the region of the stem. In what follows, an excitation spot has a Gaussian profile with a full width at half-maximum (fwhm) of 65 μm, centered in the stem part of the channel at $\mathbf{r} = (250, 250)$ μm.

The effect of patterning on the polariton condensate propagation in a microcavity with an embedded GaAs quantum well is shown in Figure 3. In the simulations, the maximum depth of the confining potential that forms the channel is set equal $U_{\mathrm{conf}}^{(\mathrm{max})} = -1$ eV. It is seen in Figure 3a that without the pattern (that is, without the confining potential in the (x, y) plane), a polariton condensate driven by the constant force F_x forms a wide trail in the direction of the force with the length >400 μm. At large distances from the excitation spot the condensate density decreases due to the finite lifetime of polaritons. The propagation of the condensate under the same conditions in the presence of a Y-shaped pattern is shown in Figure 3b. As is seen in this figure, the polariton flow propagating in the patterned microcavity is localized in the channel formed by the pattern. In the region of the junction $x \approx 500$ μm, the polariton condensate flow splits between the "upper" and "lower" branches of the Y-channel. The polariton density in the channel at the distance $x \sim 600$ μm from the source is significantly higher than that in the microcavity without the channel (*cf.* Figure 3a and b). The increase of the polariton density is caused by the confining potential that prevents the polariton flow from spreading in the (x, y) plane.

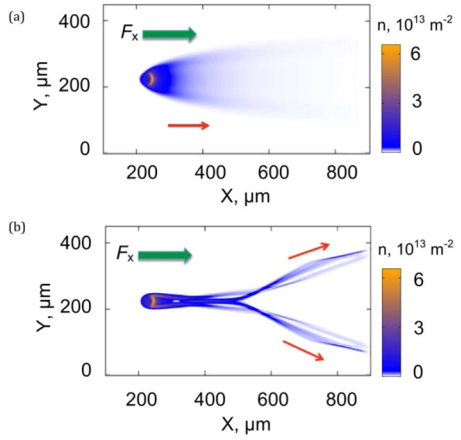

Figure 3. Propagation of the polariton condensate in a wedge-shaped microcavity with an embedded GaAs quantum well (a) without and (b) with the pattern deposited on the Bragg reflectors. The constant force acting on the polaritons in the x-direction owing to the wedge is $F_x = 13$ meV/mm. The color bar shows the polariton density $n = |\Psi(\mathbf{r}, t)|^2$. The figure shows the steady state reached after the polariton source is turned on. The polariton flux splits between the upper and lower branches of the channel in (b). Red arrows show the direction of the polariton flow.

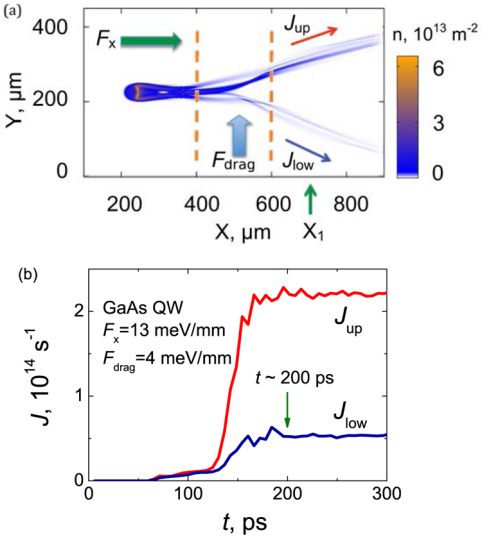

Figure 4. (a) Redistribution of the polariton flux between the upper and lower branches of the channel in response to the driving drag force F_{drag} in the region of the junction. The boundaries of a current-carrying quantum well 400 μm < x < 600 μm, in which the drag force is exerted on the polaritons, are shown by vertical dashed lines. The cross-section of the branches, at which the polariton flux J in eq 2 is determined, is labeled as x_1. (b) Dependence of the polariton flux in the upper J_{up} and lower J_{low} branches on time after the polariton source is turned on. The transient oscillations last for $t \sim 200$ ps after the source is switched on, and then the system reaches a steady state. The simulations are done for a wedge-shaped microcavity with an embedded GaAs quantum well.

To probe the effect of the drag force on the polariton flow, in addition to the constant force F_x we applied the force F_{drag} in a stripe directed in y-direction in the region of the junction. In Figure 4a the area 400 μm < x < 600 μm, in which the drag force F_{drag} is

exerted, is bounded by the dashed lines. We found in the simulations that, due to the drag, the polaritons tend to propagate in the channel in the direction of the drag force F_{drag} and therefore, they mostly move in the upper branch of the channel in Figure 4a. To characterize the redistribution of the polaritons between the upper and lower branches we calculated the total polariton flux propagating in the branch,

$$J = \int ds j_\nu(\mathbf{r}, t) \quad (2)$$

where $j_\nu(\mathbf{r}, t) \equiv \mathbf{j}(\mathbf{r}, t)\cdot\boldsymbol{\nu}$ is the component of the polariton flux density parallel to the channel, $\boldsymbol{\nu}$ is a unit vector along the branch, and

$$\mathbf{j}(\mathbf{r}, t) = \frac{\hbar}{2im}(\Psi^*(\mathbf{r}, t)\nabla\Psi(\mathbf{r}, t) - \Psi(\mathbf{r}, t)\nabla\Psi^*(\mathbf{r}, t)) \quad (3)$$

is the flux density.[45] We integrate in eq 2 over the cross section of the branch. The flux J was calculated at $x = x_1 \equiv 700\,\mu$m, that is, at a distance from the junction much larger than the width of the channel $a_{ch} \sim 60\,\mu$m.

Figure 4b shows the dependencies of the total polariton flux trough the upper (red curve) and lower (blue curve) branches as functions of time t in a microcavity with GaAs quantum well in the presence of the drag force F_{drag} = 4 meV/mm. The polariton source is turned on at the moment $t = 0$. According to the results shown in Figure 4b, the polaritons reach the point x_1 at $t \sim 60$ ps after the source is turned on. During the time interval 60 ps < t < 200 ps the polariton flux exhibits transient oscillations, and then tends to a constant value at $t \geq 200$ ps. As it follows from Figure 4b, the flux through the upper branch of the channel in the steady state is $J \approx 2.2 \times 10^{14}$ s^{-1}, which is ≈4.1× larger than that through the lower branch. Therefore, the polariton flow is redistributed among the branches in response to the drag force owing to the external, driving electric current. To quantify the redistribution of the polariton flux in the channel, we studied the dependence of the flux J on the drag force F_{drag}. It is shown in Figure 5 (left scale) that the flux in the upper branch, J_{up}, gradually increases with the rise of the drag force F_{drag}. In its turn, the flux through the lower branch, J_{low}, decreases thus, the total flux $J_{tot} = J_{up} + J_{low}$ remains approximately constant. To more fully characterize the performance of the system, we determined the fraction of the polariton flux propagating in the upper branch as follows,

$$Q = (J_{up}/J_{tot}) \times 100\% \quad (4)$$

The dependence of the fraction Q on the drag force F_{drag} for the data on the left scale of Figure 5 is shown on the right scale in the same figure. It is seen that up to 79.2% of the polariton flux propagates in the upper channel whereas only 20.8% of the flux propagates along the lower channel for the drag force F_{drag} = 4 meV/mm.

To study the effects of the channel depth on the performance of the system, we simulated the polariton

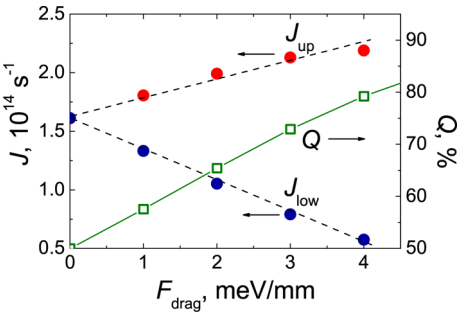

Figure 5. Redistribution of the polariton flux between the upper branch, J_{up} (red points), and lower branch, J_{low} (blue points), in response to the driving drag force F_{drag} is shown on the left scale. The polaritons fluxes in the upper and lower channel are determined at the cross-section labeled as x_1 in Figure 4a in a steady state after the transient oscillations damped. The dashed lines are shown to guide the eye. The right scale shows the fraction of the total polariton flux Q (green open squares) directed toward the upper branch, as defined in eq 4. The simulations are made for a wedge-shaped microcavity with an embedded GaAs quantum well with F_x = 13 meV/mm.

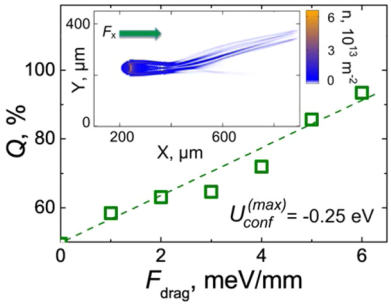

Figure 6. Redistribution of the polariton flux in the shallow channel in a wedge-shaped microcavity with an embedded GaAs quantum well. In these simulations, the maximum channel energy depth is set equal $U_{conf}^{(max)} = -0.25$ eV, which is four times smaller by absolute value than in other simulations. The inset shows the steady-state polariton distribution in the channel where the drag force F_{drag} = 6 meV/mm is applied at the junction. The color bar shows the polariton density. The main plot shows the fraction of the polariton flux running in the upper brach of the shallow channel as a function of F_{drag}. Points present the results of the simulations; the dashed line is shown to guide the eye. It is seen that the performance Q > 90% can be reached for F_{drag} = 6 meV/mm.

flow in the patterned microcavity with GaAs quantum well for different maximum channel depths $U_{conf}^{(max)}$ varied from −1 to −0.25 eV. We found that the performance of the system only weakly depends on the channel depth in this region of parameters. The results of the simulations for a "shallow" channel with $U_{conf}^{(max)} = -0.25$ eV are shown in Figure 6. It is seen in Figure 6 that as much as 93% of the total polariton flux is redistributed toward the upper branch if the drag force F_{drag} = 6 meV/mm is applied to the system.

To better understand the effects of the system size on the system performance we determined the dependence of Q on the drag force F_{drag} and on the constant force F_x for a sample, which is twice smaller than that in the above studies. In these simulations,

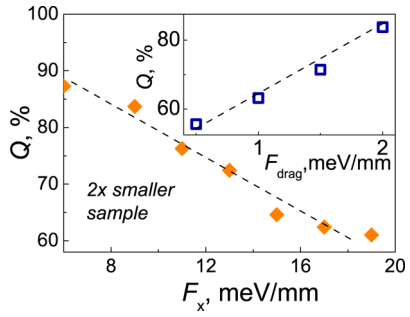

Figure 7. Performance Q of the system for a twice smaller sample. The simulations are made for a wedge-shaped microcavity with an embedded GaAs quantum well. The main plot shows the dependence of Q on the constant accelerating force F_x for fixed drag force F_{drag} = 2 meV/mm. The inset shows the dependence of Q on F_{drag} for F_x = 9 meV/mm. The points show the results of the simulations, the lines are shown to guide the eye. It is seen that the performance $Q \sim 90\%$ can be reached in a smaller sample for lower F_x force.

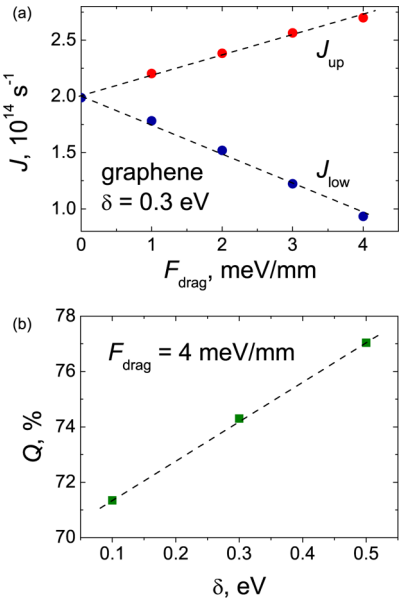

Figure 8. (a) Redistribution of the polariton flux between the upper and lower branches in response to the magnitude of the driving drag force F_{drag} in a microcavity with an embedded gapped graphene layer. The polariton fluxes in the upper and lower branches, J_{up} and J_{low}, are determined at the cross-section with the same x-coordinate (x_1) as for the microcavity with GaAs quantum well. (b) Performance of the system Q, eq 4, as a function of the energy gap in graphene. It is seen that up to 77% of polaritons are propagating through the upper channel if the drag force F_{drag} = 4 meV/mm is applied at the junction.

all geometrical sizes of the channel were reduced twice including the total channel length, the channel width, and the width of the current-carrying quantum well. The polariton fluxes J_{up} and J_{low} in the upper and lower channels were determined at the cross-section x_1 positioned at the distance of 100 μm from the junction, to keep the same distance-to-channel width ratio. However, to avoid the effects related to the numerical accuracy, we kept the numerical box size the same as in the previous simulations.

We found that in the small channel, high-enough performance Q can be reached for smaller drag forces F_{drag}. The system demonstrates the increase of the fraction Q from 55.6 to 83.7% when F_{drag} varies from 0.5 to 2 meV/mm at fixed F_x = 9 meV/mm, as is shown in the inset in Figure 7. On the other hand, the fraction of the polaritons in the upper channel gradually decreases from 87.3 to 61.0% with the increase of the constant force F_x from 6 to 19 meV/mm for fixed F_{drag} = 2 meV/mm (see the main plot in Figure 7). This can be understood as follows. For small F_x, the acceleration of the polaritons due to the microcavity wedge shape is small and hence, the polariton flow velocities at the junction are relatively low. Thus, even a small drag force can effectively redistribute the polariton flux between the channels. At high F_x, the polariton velocity at the junction increases and the effectiveness of the system for small drags drops. Thus, there is an optimum set of parameters (F_x, F_{drag}) that provides the maximum performance Q of the system.

In all simulations above, we studied the polariton flow in a patterned microcavity with an embedded GaAs quantum well. To understand the effects of the material properties on the polariton dynamics, we also simulated the flow of a polariton condensate in a microcavity with an embedded graphene layer. The parameters are detailed in the Methodology section. For an embedded gapped graphene layer, the polariton mass and the speed of sound in the condensate can be tuned by changing the energy gap in the quasiparticle excitation spectrum δ. The redistribution of the polariton flux in a "large" channel (identical to that in Figure 3) is shown in Figure 8a for the energy gap δ = 0.3 eV. It is seen that the response of the system to the applied drag force is similar to that for an embedded GaAs quantum well (*cf.* Figure 5). We studied the dependence of the polariton fraction Q in the upper channel on the energy gap δ keeping the forces F_x and F_{drag} fixed. In these simulations, we varied the gap δ from 0.1 to 0.5 eV that corresponds to the experimentally accessible range.[41−43,46] It is shown in Figure 8b that the performance of the system grows with the increase of the energy gap δ, and it reaches ~77% for the maximum gap δ = 0.5 eV. Thus, a patterned microcavity with an embedded graphene layer at high energy gap ~0.5 eV demonstrates the performance comparable with that for a microcavity with an embedded GaAs quantum well.

Finally, to estimate the response speed of the system, we studied the transient dynamics of a polariton condensate in the channel when the direction of the driving current is inverted. The main plot in Figure 9 shows the obtained results for a microcavity with GaAs quantum well. In these simulations, we waited for t = 273 ps after the pumping was turned on until the system reached an equilibrium in the presence of a

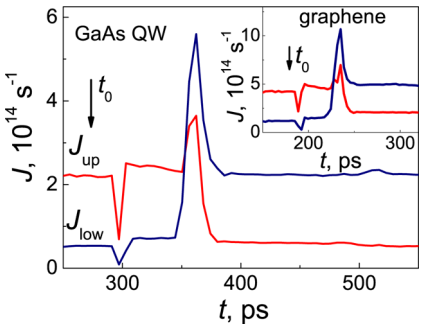

Figure 9. Main plot: Response of the system to switching direction of the drag force in a microcavity with an embedded GaAs quantum well. The drag is directed toward the upper channel at $t < t_0 = 273$ ps after the source is turned on; the polaritons mostly propagate *via* the upper branch. The direction of the drag is changed to opposite at $t = t_0$, and then the transient oscillations of the polariton flux occur for ~110 ps. After the oscillations are damped, most of polaritons propagate *via* the lower branch. The red curve shows the time dependence of the polariton flux in the upper branch, and the blue curve shows the same dependence in the lower branch. The simulations are made for F_x = 13 meV/mm and F_{drag} = 4 meV/mm. The inset shows the same dependence calculated for a microcavity with an embedded graphene layer with the energy gap δ = 0.5 eV. In this case, t_0 = 180 ps and the transient oscillations last for ~70 ps after the direction of the drag was changed.

drag force. In this steady state, the polaritons mostly propagated in the upper channel, in accordance with our previous consideration. At $t = t_0 \equiv 273$ ps, we changed the direction of the drag force to opposite. Since the drag force now pushes the polaritons down in the junction area, the polaritons tend to propagate *via* the lower channel, whereas the flux through the upper channel decreases. After the transient oscillations were damped, the system came to a new equilibrium state where most of the polaritons propagated through the lower channel. The spike on the curves at $t \sim 300$ ps is caused by the arrival of the precursor wave, which is the shock-like disturbance of the polariton condensate density propagating with a sound velocity from the region of the junction. According to Figure 9 (main plot), the characteristic switching time of the system between the two states where the polaritons propagate *via* the upper and lower branches is $t_{sw} \approx$ 110 ps. This means that the maximum switch frequency for this junction can reach $f = t_{sw}^{-1} \approx 9.1$ GHz at the given linear size of the system. The inset in Figure 9 shows the same dependence as in the main plot, but calculated for a microcavity with gapped graphene at δ = 0.5 eV. In this case, the moment at which the direction of the drag is reversed is $t_0 = 180$ ps. It is seen that the transient oscillations in the microcavity with graphene are damped after $t_{sw} \approx 70$ ps. Thus, the maximum switch frequency for the switch with graphene can reach $f \approx 14$ GHz at the given linear size of the system. The higher response speed for a microcavity with graphene is caused by lower effective mass (and hence, higher mobility) of polaritons.

Polariton Switch in a Flat Microcavity. We now consider another design of the polariton switch based on the drag effect. In this case, the reflectors are parallel to each other. In such a "flat" microcavity the only force acting on the polaritons is the drag force due to the interactions with the current. Flat microcavities are widely used in the studies of exciton polaritons in semiconductor heterostructures.[38,39]

In this design, the microcavity has no decoration. The Y-shaped channel is formed by the stripes made of semiconductor quantum wells or gapped graphene.[47] While the design of a nanojunction of the graphene stripes is technologically challenging, the possibility of fabrication of a junction of graphene stripes with help of the covalent functionalization has recently been proposed.[48] We note that the utility of electric splitters based on graphene structures has recently been discussed in the literature.[49] The current-carrying quantum well is now also Y-shaped; that is, its shape is identical to the channel shape. Similarly to the design above, the excitons in the quantum well or gapped graphene structure are excited due to the laser pumping at the stem of the channel. The main concept is schematically illustrated in Figure 2.

The voltage V is applied across the electron quantum well between the stem and one of the branches. The polaritons are formed by excitons and cavity photons and are dragged by the electron current in the electron quantum well along one of the branches. The direction of the electric current and, hence, of the polariton flux is defined by the electric switch S (see Figure 2). If the switch S is closed in position A then, the electric current in the electron quantum well runs along the upper branch. Because of the drag effect caused by the interactions between the excitons and the electrons,[11,12] the electron current induces the flow of polariton quasiparticles in the cavity along the upper branch. Then, if the switch is closed in position B, the flow of polariton quasiparticles propagates along the lower branch. Thus, the path of the polaritons in the Y-shaped channel can be dynamically changed by changing the position of the switch S.

The switch can also be completely locked by closing both positions A and B and changing the polarity of the driving source V. In this case, the electron current (and hence, the drag force) is directed toward the stem and prevents the polaritons from spreading in the channel. As a result, the polaritons are localized in the region of the excitation spot in the stem, and the switch is locked.

The flux density **j** of the polariton superfluid in the channel is given by eq 1. For the polaritons velocities smaller than the speed of sound c_s in the polariton superfluid, the polariton flux density can be found as follows[12]

$$\mathbf{j} \equiv n_n v = \gamma \mathbf{E} \qquad (5)$$

where n_n is the density of the normal component in the polariton subsystem formed by the quasiparticles, and v is the average velocity of the dragged polariton quasiparticles. Estimating the magnitude of the electric field as $|\mathbf{E}| \simeq V/L$, where V is the voltage across the channel and L is the length of the channel, one obtains for the magnitude of the averaged polariton velocity

$$v = \frac{\gamma V}{n_n L} \tag{6}$$

The time t, required for a quasiparticle to propagate across the channel, is estimated as

$$t \simeq \frac{L}{v} = \frac{n_n L^2}{\gamma V} \tag{7}$$

In the relevant parameter range (see Methodology), eq 7 gives the estimate $t \approx 49$ ps for the polariton propagation time in the channel of the total length $L = 30$ μm with GaAs quantum well for the voltage $V = 8$ mV. The average velocity of the polariton quasiparticles calculated from eq 6 in this case is $v \approx 6.1 \times 10^5$ m/s, which is smaller than the sound velocity in the polariton superfluid $c_s = 7.4 \times 10^5$ m/s. Therefore, the breakdown of superfluidity in the system does not occur.[8] For a shorter channel of length $L = 10$ μm, the polariton propagation time is reduced to $t = 15$ ps and the velocity is $v \approx 6.9 \times 10^5$ m/s for the voltage $V = 3$ mV. For higher voltage $V = 5$ mV, the propagation time becomes as short as 9 ps; however, the polariton velocity $v = 1.1 \times 10^6$ m/s exceeds the sound velocity c_s; thus, the superfluidity breakdown should occur under these conditions.[8] In this case, the polariton flow at low densities can be seen as a propagation of a normal polariton gas along the channel.

In the case of a microcavity with embedded graphene with the energy gap $\delta = 0.2$ eV, the sound velocity is increased to $c_s = 2.6 \times 10^6$ m/s. For a 30 μm-long channel and $V = 7$ meV the propagation time is 35 ps, and the average polariton velocity is 8.7×10^5 m/s. For graphene with $\delta = 0.5$ eV, one has $c_s = 7.3 \times 10^5$ m/s, which is similar to that in a condensate in a GaAs-based microcavity. For the same parameters $L = 30$ μm and $V = 7$ meV, one obtains $t = 43$ ps and $v = 7.0 \times 10^5$ m/s that again lies in the experimentally accessible range.

From the above estimates it follows that polaritons with the lifetime $\tau \sim 50$ ps can be utilized to design the switch. The most favorable conditions for the observation of the superfluid polariton flow in the channel can be achieved at high polariton densities n, that is, at relatively high sound velocities $c_s \propto \sqrt{n}$.

CONCLUSIONS

In the above studies we considered two designs of an electrically controlled optical switch. In both cases, we focused on the propagation of polaritons, which are a quantum superposition of cavity photons and excitons. A significant challenge is designing a system where the direction of the polariton flow is controlled by means of the electrical current since both photons and excitons are electrically neutral. In our studies, to control the polariton propagation we utilize the drag effect, which is the entrainment of polaritons by an electric current running in the neighboring quantum well. Recently, the drag of polaritons by the electric current in an unrestricted planar microcavity has been considered theoretically. In the above studies, we utilize this approach to design the nanostructures, in which the polaritons are localized in a circuit made by quasi-one-dimensional polariton wires.

In the first setup, the polaritons propagate in the Y-shaped channel due to a constant force created in a wedge-shaped microcavity. In this case, the controlling drag force is directed perpendicularly to the direction of the stem of the channel and it pushes the polaritons in one of the two branches. Changes in the direction of the electric current results in switching of the path in which the polaritons propagate.

In the second setup, the polaritons in a flat microcavity are considered. In this case, the constant force is absent and the polaritons are only dragged by an electric current running in a Y-shaped quantum well. The latter setup is more technologically challenging, mostly due to the requirement of a high-quality junction, however, this scheme provides additional advantages for the polariton flow control. Specifically, the magnitude of the polariton flow can be tuned by setting the voltage across the channel to a given value. In both designs, the propagation of polariton condensate in a microcavity with embedded graphene with the energy gap $\delta = 0.5$ eV is similar to that in a microcavity with a GaAs quantum well. Therefore, our simulations demonstrate that the performances of the system with gapped graphene and with a GaAs quantum well are close to each other. However, due to small effective mass of the quasiparticles in gapped graphene, the response speed for the switch with an embedded graphene is about 1.5× higher that that for a microcavity with a GaAs quantum well. We suggest that faster response speed of the switches with graphene might be one of the factors that will stimulate the investigations in this direction.

The simulations are done for polaritons with the lifetime $\tau = 100$ ps. Such long-lifetime polaritons have recently been obtained in GaAs-based microcavities.[15] However, our estimates show that polaritons with the lifetime $\tau \sim 50$ ps can also be utilized in the proposed switches.

The optical switches with microcavity polariton condensate can be applied as a basic element of optical logic circuits.[25−27] The setup that we proposed in this paper improves the flexibility of the device functions

since it can be used as a standard optical transistor with on and off functions as well as a two- or multiway router that directs the optical signals to the ultimate destination.

METHODOLOGY

The dynamics of the polariton condensate were captured *via* the nonequilibrium Gross-Pitaevskii equation for the condensate wave function $\Psi(\mathbf{r}, t)$[39]

$$i\hbar\frac{\partial\Psi(\mathbf{r},t)}{\partial t} = -\frac{\hbar^2}{2m}\Delta\Psi(\mathbf{r},t) + U(\mathbf{r},t)\Psi(\mathbf{r},t) + g\Psi(\mathbf{r},t)|\Psi(\mathbf{r},t)|^2 - \frac{i\hbar}{2\tau}\Psi(\mathbf{r},t) + iP(\mathbf{r}) \quad (8)$$

where m is the polariton mass, $\mathbf{r} = (x, y)$ is a two-dimensional vector in the plane of the microcavity, t is time, g is the polariton−polariton interaction strength, τ is the polariton lifetime, and the source terms $P(\mathbf{r})$ describes incoherent laser pumping of the polariton reservoir. In our simulations, we set $\tau = 100$ ps.[15]

The effective potential for the polaritons

$$U(\mathbf{r},t) = U_{\text{conf}}(\mathbf{r}) + U_{\text{w}}(\mathbf{r}) + U_{\text{ex}}(\mathbf{r},t) + U_{\text{drag}}(\mathbf{r},t) \quad (9)$$

is the sum of the confining potential owing to microcavity patterning $U_{\text{conf}}(\mathbf{r})$, a linear potential corresponding to a constant accelerating force in a wedge-shaped microcavity $U_{\text{w}}(\mathbf{r})$, the interactions of polaritons with a cloud of uncoupled excitons created by the laser radiation $U_{\text{ex}}(\mathbf{r}, t)$, and a time-dependent drag potential $U_{\text{drag}}(\mathbf{r}, t)$ caused by the driving electric current. The confining potential $U_{\text{conf}}(\mathbf{r})$ that forms the Y-shaped channel is shown in Figure 1b. We varied the depth of the channel compared to zero value outside the waveguide from $U_{\text{conf}}^{(\max)} = -1$ to -0.25 eV.[16−18] Account of the interactions of polaritons with the excitons is important for the polariton dynamics.[50] The respective potential $U_{\text{ex}}(\mathbf{r}, t)$ was set in a Gaussian form with fwhm of 65 μm and height of 5 meV. The average force acting upon a polariton wave packet in a wedge-shaped microcavity is $\mathbf{F}(\mathbf{r}) = -\nabla E_C(\mathbf{r})$, where $E_C(\mathbf{r})$ is the energy of the polariton band taken at the in-plane wavevector of the polariton $\mathbf{k} = 0$.[14,15] For the wedge-like microcavity considered in this paper, the energy $E_C(\mathbf{r})$ is a linear function of the spatial coordinate thus, the force is coordinate-independent. The corresponding potential is

$$U_{\text{w}}(\mathbf{r}) = -F_x x \quad (10)$$

where $F_x = |\partial E_C(\mathbf{r})/\partial x|$, and we suppose that the force is applied in x-direction, along the stem of the Y-shaped channel.

The potential that represents the drag force in y-direction is taken equal

$$U_{\text{drag}}(\mathbf{r},t) = -F_{\text{drag}}(t)y \quad (11)$$

in a stripe 400 μm $< x <$ 600 μm and $U_{\text{drag}}(\mathbf{r}, t) = 0$ otherwise. The drag force exerted on polaritons by charges moving in a neighboring quantum well is estimated in the τ-approximation as

$$F_{\text{drag}}(t) = \frac{\langle p\rangle}{\tau_p} = \frac{m\gamma E(t)}{n_n\tau_p} \quad (12)$$

where $\langle p\rangle$ is the average gain of the linear momentum of polaritons owing to the drag, τ_p is the polariton momentum relaxation time, $E(t)$ is a time-dependent electric field applied in the plane of the quantum well with free electrons,

$$n_n = \frac{3\zeta(3)s(k_{\text{B}}T)^3}{2\pi\hbar^2c_s^4m} \quad (13)$$

is the density of the normal component in a polariton superfluid,[51] $\zeta(3) \approx 1.202$ is the Riemann zeta function, $s = 4$ is the spin degeneracy factor, k_{B} is the Boltzmann constant, T is temperature, and $c_s = (gn/m)^{1/2}$ is the sound velocity in the spectrum of collective excitations in the polaritonic system.

The polariton effective mass is[52]

$$m = 2(m_{\text{ex}}^{-1} + cL_C/\sqrt{\varepsilon}\pi\hbar)^{-1} \quad (14)$$

where m_{ex} is the exciton effective mass, L_C is the length of the microcavity, ε is the dielectric constant of the microcavity, and c is the speed of light in vacuum. In the simulations for a GaAs-based microcavity, we set $\varepsilon = 13$ and $m_{\text{ex}} = m_{\text{e}} + m_{\text{h}} = 0.24m_0$, where $m_{\text{e}} = 0.07m_0$ and $m_{\text{h}} = 0.17m_0$ are the electron and hole effective masses, respectively, and m_0 is the free electron mass. We consider the case of zero detuning where the cavity photons and the excitons are in the resonance at $\mathbf{k} = 0$. In this case, the length of the microcavity is[52]

$$L_C = \frac{\pi\hbar c}{\sqrt{\varepsilon}(E_{\text{band}} - E_{\text{binding}})} \quad (15)$$

where where E_{band} is the band gap energy and E_{binding} is the binding energy of a 2D exciton. In GaAs/AlGaAs quantum wells we set $E_{\text{band}} = 1.51$ eV and $E_{\text{binding}} = 7$ meV.[53]

Formation of the excitons in graphene requires a gap in the electron and hole excitation spectra, which can be created and dynamically tuned by applying an external electric field in the direction normal to the graphene layer.[41−43] The gap can also be opened by chemical doping of graphene.[46] The polariton mass m and the interaction strength g in gapped graphene depend on the energy gap δ. For the gapped graphene one has $E_{\text{band}} = 2\delta$ and $E_{\text{binding}} = V_0 - C/\delta^2$, that results in the following[9]

$$L_C = \frac{\pi\hbar c}{\sqrt{\varepsilon}(2\delta - V_0 + C/\delta^2)} \quad (16)$$

where $V_0 = e^2/4\pi\varepsilon\varepsilon_0 r'$, $C = (\hbar e v_{\text{F}})^2/8\pi\varepsilon\varepsilon_0 r'^3$, e is the absolute value of the electron charge, ε_0 is the permittivity of free space, and $v_{\text{F}} \approx 10^6$ m/s is the Fermi-velocity of the electrons in graphene. The parameter r' is found from the equation

$$2\delta^2(2\delta - \hbar\omega)r'^3 - 2q\delta^2 r'^2 + q(\hbar v_{\text{F}})^2 = 0 \quad (17)$$

where $q = e^2/4\pi\varepsilon\varepsilon_0$. For dipolar excitons in GaAs/AlGaAs coupled quantum wells, the energy of the recombination peak is $\hbar\omega = 1.61$ eV.[54] We expect similar photon energies in graphene. However, its exact value depends on the graphene dielectric environment and substrate properties. The exciton effective mass in gapped graphene is[9]

$$m_{\text{ex}} = \frac{2\delta^4}{Cv_{\text{F}}^2} \quad (18)$$

The polariton−polariton interaction strength is[55]

$$g = \frac{3e^2a_{\text{B}}}{8\pi\varepsilon_0\varepsilon} \quad (19)$$

where $a_{\text{B}} = 2\pi\varepsilon_0\varepsilon\hbar^2/m_{\text{r}}e^2$ is the two-dimensional Bohr radius of the exciton and m_{r} is the exciton reduced mass. For GaAs/AlGaAs quantum wells we set $m_{\text{r}} = m_{\text{e}}m_{\text{h}}/(m_{\text{e}} + m_{\text{h}})$. The exciton reduced mass in gapped graphene was set equal $m_{\text{r}} = (1/4)m_{\text{ex}}$.[9]

Following ref 12 it is easy to obtain that the drag coefficient γ' in graphene is connected with the drag coefficient γ in a GaAs quantum well *via* the following equation

$$\gamma' = \gamma\left(\frac{e^z - 1}{e^{z'} - 1}\right)^2 e^{z' - z} \quad (20)$$

where $z = gn/k_{\text{B}}T$, and the parameters that relate to graphene are marked with prime.

By taking the polariton condensate density $n = 10^{14}$ m^{-2}, the separation between GaAs quantum wells $D = 17.5$ nm,

the drag coefficient $\gamma = 6 \times 10^{16}$ (Vs)$^{-1}$ and the relaxation time $\tau_p = 6 \times 10^{-11}$ s as representative parameters for temperature $T = 10$ K,[12,56–58] from eqs 12–15 and 19 one obtains $n_n = 2.6 \times 10^{13}$ m^{-1} and the drag force $F_{drag} = 0.17–8.3$ meV/mm for the working range of electric fields $E = 0.01–0.5$ V/mm. For the structure that encompasses a gapped graphene layer we expect similar τ_p. For graphene at $\delta = 0.2$ eV and $D = 17.5$ nm, eqs 12–14 and 16–20 give $n_n = 3.5 \times 10^{11}$ m^{-1}, $\gamma' = 1.3 \times 10^{15}$ (V s)$^{-1}$ and $F_{drag} = 0.13–6.6$ meV/mm for the same range of electric fields $E = 0.01–0.5$ V/mm. For graphene at $\delta = 0.5$ eV, one obtains $n_n = 3.5 \times 10^{13}$ m^{-1}, $\gamma' = 1.1 \times 10^{17}$ (Vs)$^{-1}$ and the drag force $F_{drag} = 0.17–8.3$ meV/mm for the same range of electric fields and D. We restrict our consideration to the case where the response of the system to the drag is linear (*cf.* Figures 5 and 8a), and hence, eq 1 is applicable.

The numerical code we devised for the simulations is available for researchers upon request.

Conflict of Interest: The authors declare no competing financial interest.

Acknowledgment. The authors are gratefully acknowledge support from Army Research Office, Grant #64775-PH-REP. G.V.K. is also grateful for support to Professional Staff Congress-City University of New York, Award #66140-0044. The authors are grateful to the Center for Theoretical Physics of New York City College of Technology of the City University of New York for providing computational resources.

REFERENCES AND NOTES

1. Gibbs, H. M., Khitrova, G., Peyghambarian, N., Eds.; *Nonlinear Photonics*; Springer: London, 2011.
2. Deng, H.; Weihs, G.; Snoke, D.; Bloch, J.; Yamamoto, Y. Polariton Lasing *vs.* Photon Lasing in a Semiconductor Microcavity. *Proc. Natl. Acad. Sci. U. S. A.* **2002**, *100*, 15318–15323.
3. Amo, A.; Liew, T. C. H.; Adrados, C.; Houdre, R.; Giacobino, E.; Kavokin, A. V.; Bramati, A. Exciton-Polariton Spin Switches. *Nat. Photonics* **2010**, *4*, 361–366.
4. Liew, T. C. H.; Kavokin, A. V.; Ostatnicky, T.; Kaliteevski, M.; Shelykh, I. A.; Abram, R. A. Exciton-Polariton Integrated Circuits. *Phys. Rev. B: Condens. Matter Mater. Phys.* **2010**, *82*, 033302.
5. Menon, V. M.; Deych, L. I.; Lisyansky, A. A. Nonlinear Optics: Towards Polaritonic Logic Circuits. *Nat. Photonics* **2010**, *4*, 345–346.
6. Carusotto, I.; Ciuti, C. Probing Microcavity Polariton Superfluidity Through Resonant Rayleigh Scattering. *Phys. Rev. Lett.* **2004**, *93*, 166401.
7. Amo, A.; Lefrere, J.; Pigeon, S.; Adrados, C.; Ciuti, C.; Carusotto, I.; Houdre, R.; Giacobino, E.; Bramati, A. Superfluidity of Polaritons in Semiconductor Microcavities. *Nat. Phys.* **2009**, *5*, 805–810.
8. Wouters, M.; Savona, V. Superfluidity of a Nonequilibrium Bose–Einstein Condensate of Polaritons. *Phys. Rev. B: Condens. Matter Mater. Phys.* **2010**, *81*, 054508.
9. Berman, O. L.; Kezerashvili, R. Ya.; Ziegler, K. Superfluidity and Collective Properties of Excitonic Polaritons in Gapped Graphene in a Microcavity. *Phys. Rev. B: Condens. Matter Mater. Phys.* **2012**, *86*, 235404.
10. Wouters, M.; Carusotto, I. Superfluidity and Critical Velocities in Nonequilibrium Bose–Einstein Condensates. *Phys. Rev. Lett.* **2010**, *105*, 020602.
11. Berman, O. L.; Kezerashvili, R. Ya.; Lozovik, Yu. E. Can We Move Photons? *Phys. Lett. A* **2010**, *374*, 3681–3684.
12. Berman, O. L.; Kezerashvili, R. Ya.; Lozovik, Yu. E. Drag Effects in a System of Electrons and Microcavity Polaritons. *Phys. Rev. B: Condens. Matter Mater. Phys.* **2010**, *82*, 125307.
13. Lozovik, Yu. E.; Nikitkov, M. Drag Effects in a Two-Layer System of Spatially Separated Electrons and Excitons. *J. Exp. Theor. Phys.* **1997**, *84*, 612–618.
14. Sermage, B.; Malpuech, G.; Kavokin, A. V.; Thierry-Mieg, V. Polariton Acceleration in a Microcavity Wedge. *Phys. Rev. B: Condens. Matter Mater. Phys.* **2001**, *64*, 081303(R).
15. Nelsen, B.; Liu, G.; Steger, M.; Snoke, D. W.; Balili, R.; West, K.; Pfeiffer, L. Dissipationless Flow and Sharp Threshold of a Polariton Condensate with Long Lifetime. *Phys. Rev. X* **2013**, *3*, 041015.
16. Lai, C. W.; Kim, N. Y.; Utsunomiya, S.; Roumpos, G.; Deng, H.; Fraser, M. D.; Byrnes, T.; Recher, P.; Kumada, N.; Fujisawa, T.; *et al.* Coherent Zero-State and π-State in an Exciton-Polariton Condensate Array. *Nature* **2007**, *450*, 529–532.
17. Daïf, O. E.; Baas, A.; Guillet, T.; Brantut, J.-P.; Kaitouni, R. I.; Staehli, J. L.; Morier-Genoud, F.; Deveaud, B. Polariton Quantum Boxes in Semiconductor Microcavities. *Appl. Phys. Lett.* **2006**, *88*, 061105.
18. Kaitouni, R. I.; Daïf, O. E.; Baas, A.; Richard, M.; Paraiso, T.; Lugan, P.; Guillet, T.; Morier-Genoud, F.; Ganière, J. D.; Staehli, J. L.; *et al.* Engineering the Spatial Confinement of Exciton Polaritons in Semiconductors. *Phys. Rev. B: Condens. Matter Mater. Phys.* **2006**, *74*, 155311.
19. Das, A.; Bhattacharya, P.; Heo, J.; Banerjee, A.; Guo, W. Polariton Bose–Einstein Condensate at Room Temperature in an Al(Ga)N Nanowire-Dielectric Microcavity with a Spatial Potential Trap. *Proc. Natl. Acad. Sci. U. S. A.* **2013**, *110*, 2735–2740.
20. Wertz, E.; Ferrier, L.; Solnyshkov, D. D.; Johne, R.; Sanvitto, D.; Lemaitre, A.; Sagnes, I.; Grousson, R.; Kavokin, A. V.; Senellart, P.; *et al.* Spontaneous Formation and Optical Manipulation of Extended Polariton Condensates. *Nat. Phys.* **2010**, *6*, 860–864.
21. Van Vugt, L. K.; Piccione, B.; Cho, C.-H.; Nukala, P.; Agarwal, R. One-Dimensional Polaritons with Size-Tunable and Enhanced Coupling Strengths in Semiconductor Nanowires. *Proc. Natl. Acad. Sci. U. S. A.* **2011**, *108*, 10050–10055.
22. Nguyen, H. S.; Vishnevsky, D.; Sturm, C.; Tanese, D.; Solnyshkov, D.; Galopin, E.; Lemaître, A.; Sagnes, I.; Amo, A.; Malpuech, G.; *et al.* Realization of a Double-Barrier Resonant Tunneling Diode for Cavity Polaritons. *Phys. Rev. Lett.* **2013**, *110*, 236601.
23. Boulier, T.; Bamba, M.; Amo, A.; Adrados, C.; Lemaitre, A.; Galopin, E.; Sagnes, I.; Bloch, J.; Ciuti, C.; Giacobino, E.; *et al.* Polariton-Generated Intensity Squeezing in Semiconductor Micropillars. *Nat. Commun.* **2014**, *5*, 3260.
24. Miller, D. A. B. Are Optical Transistors the Logical Next Step?. *Nat. Photonics* **2010**, *4*, 3–5.
25. Gao, T.; Eldridge, P. S.; Liew, T. C. H.; Tsintzos, S. I.; Stavrinidis, G.; Deligeorgis, G.; Hatzopoulos, Z.; Savvidis, P. G. Polariton Condensate Transistor Switch. *Phys. Rev. B: Condens. Matter Mater. Phys.* **2012**, *85*, 235102.
26. Ballarini, D.; De Giorgi, M.; Cancellieri, E.; Houdré, R.; Giacobino, E.; Cingolani, R.; Bramati, A.; Gigli, G.; Sanvitto, D. All-Optical Polariton Transistor. *Nat. Commun.* **2013**, *4*, 1778.
27. Snoke, D. Microcavity Polaritons: A New Type of Light Switch. *Nat. Nanotechnol.* **2013**, *8*, 393–395.
28. Bajoni, D.; Semenova, E.; Lemaitre, A.; Bouchoule, S.; Wertz, E.; Senellart, P.; Barbay, S.; Kuszelewicz, R.; Bloch, J. Optical Bistability in a GaAs-Based Polariton Diode. *Phys. Rev. Lett.* **2008**, *101*, 266402.
29. Lilly, M. P.; Eisenstein, J. P.; Pfeiffer, L. N.; West, K. W. Coulomb Drag in the Extreme Quantum Limit. *Phys. Rev. Lett.* **1998**, *80*, 1714–1717.
30. Seamons, J. A.; Morath, C. P.; Reno, J. L.; Lilly, M. P. Coulomb Drag in the Exciton Regime in Electron-Hole Bilayers. *Phys. Rev. Lett.* **2009**, *102*, 026804.
31. Cage, M. E.; Field, B. F.; Dziuba, R. F.; Girvin, S. M.; Gossard, A. C.; Tsui, D. C. Temperature Dependence of the Quantum Hall Resistance. *Phys. Rev. B: Condens. Matter Mater. Phys.* **1984**, *30*, 2286–2288.
32. Balili, R.; Nelsen, B.; Snoke, D. W.; Pfeiffer, L.; West, K. Role of the Stress Trap in the Polariton Quasiequilibrium Condensation in GaAs Microcavities. *Phys. Rev. B: Condens. Matter Mater. Phys.* **2009**, *79*, 075319.
33. Butov, L. Exciton Condensation in Coupled Quantum Wells. *Solid State Commun.* **2003**, *127*, 89–98.
34. Kasprzak, J.; Richard, M.; Kundermann, S.; Baas, A.; Jeambrun, P.; Keeling, J. M. J.; Marchetti, F. M.; Szymanska, M. H.; Andre, R.; Staehli, J. L.; *et al.* Bose–Einstein

Condensation of Exciton Polaritons. *Nature* **2006**, *443*, 409–414.
35. Wu, S.; Buckley, S.; Jones, A. M.; Ross, J. S.; Ghimire, N. J.; Yan, J.; Mandrus, D. G.; Yao, W.; Hatami, F.; Vuckovic, J.; *et al.* Control of Two-Dimensional Excitonic Light Emission *via* Photonic Crystal. *2D Materials* **2014**, *1*, 011001.
36. Furchi, M.; Urich, A.; Pospischil, A.; Lilley, G.; Unterrainer, K.; Detz, H.; Klang, P.; Andrews, A. M.; Schrenk, W.; Strasser, G.; *et al.* Microcavity-Integrated Graphene Photodetector. *Nano Lett.* **2012**, *12*, 2773–2777.
37. Youngblood, N.; Anugrah, Y.; Ma, R.; Koester, S. J.; Li, M. Multifunctional Graphene Optical Modulator and Photodetector Integrated on Silicon Waveguides. *Nano Lett.* **2014**, *14*, 2741–2746.
38. Deng, H.; Haug, H.; Yamamoto, Y. Exciton-Polariton Bose–Einstein Condensation. *Rev. Mod. Phys.* **2010**, *82*, 1489–1537.
39. Carusotto, I.; Ciuti, C. Quantum Fluids of Light. *Rev. Mod. Phys.* **2013**, *85*, 299–366.
40. Berman, O. L.; Kezerashvili, R. Ya.; Lozovik, Yu. E.; Snoke, D. W. Bose–Einstein Condensation and Superfluidity of Trapped Polaritons in Graphene and Quantum Wells Embedded in a Microcavity. *Philos. Trans. R. Soc., A* **2010**, *368*, 5459–5482.
41. Kuzmenko, A. B.; Crassee, I.; van der Marel, D.; Blake, P.; Novoselov, K. S. Determination of the Gate-Tunable Band Gap and Tight-Binding Parameters in Bilayer Graphene Using Infrared Spectroscopy. *Phys. Rev. B: Condens. Matter Mater. Phys.* **2009**, *80*, 165406.
42. Mak, K. F.; Lui, C. H.; Shan, J.; Heinz, T. F. Observation of an Electric-Field-Induced Band Gap in Bilayer Graphene by Infrared Spectroscopy. *Phys. Rev. Lett.* **2009**, *102*, 256405.
43. Zhang, Y.; Tang, T.-T.; Girit, C.; Hao, Z.; Martin, M. C.; Zettl, A.; Crommie, M. F.; Shen, Y. R.; Wang, F. Direct Observation of a Widely Tunable Bandgap in Bilayer Graphene. *Nature* **2009**, *459*, 820–823.
44. Song, J. C. W.; Abanin, D. A.; Levitov, L. S. Coulomb Drag Mechanisms in Graphene. *Nano Lett.* **2013**, *13*, 3631–3637.
45. Messiah, A. *Quantum Mechanics; Series in Physics*; Interscience: New York, 1961.
46. Haberer, D.; Vyalikh, D. V.; Taioli, S.; Dora, B.; Farjam, M.; Fink, J.; Marchenko, D.; Pichler, T.; Ziegler, K.; Simonucci, S.; *et al.* Tunable Band Gap in Hydrogenated Quasi-Free-Standing Graphene. *Nano Lett.* **2010**, *10*, 3360–3366.
47. Berger, C.; Song, Z.; Li, X.; Wu, X.; Brown, N.; Naud, C.; Mayou, D.; Li, T.; Hass, J.; Marchenkov, A. N.; *et al.* Electronic Confinement and Coherence in Patterned Epitaxial Graphene. *Science* **2006**, *312*, 1191–1196.
48. Cocchi, C.; Ruini, A.; Prezzi, D.; Caldas, M. J.; Molinari, E. Designing All-Graphene Nanojunctions by Covalent Functionalization. *J. Phys. Chem. C* **2011**, *115*, 2969–2973.
49. Zhu, X.; Yan, W.; Mortensen, N. A.; Xiao, S. Bends and Splitters in Graphene Nanoribbon Waveguides. *Opt. Express* **2013**, *21*, 3486–3491.
50. Fernandez, Y. N.; Vasilevskiy, M. I.; Trallero-Giner, C.; Kavokin, A. Condensed Exciton Polaritons in a Two-Dimensional Trap: Elementary Excitations and Shaping by a Gaussian Pump Beam. *Phys. Rev. B: Condens. Matter Mater. Phys.* **2013**, *87*, 195441.
51. Berman, O. L.; Kezerashvili, R. Ya.; Ziegler, K. Superfluidity of Dipole Excitons in the Presence of Band Gaps in Two-Layer Graphene. *Phys. Rev. B: Condens. Matter Mater. Phys.* **2012**, *85*, 035418.
52. Berman, O. L.; Lozovik, Yu. E.; Snoke, D. W. Theory of Bose–Einstein Condensation and Superfluidity of Two-Dimensional Polaritons in an In-Plane Harmonic Potential. *Phys. Rev. B: Condens. Matter Mater. Phys.* **2008**, *77*, 155317.
53. Dingle, R.; Wiegmann, W.; Henry, C. H. Quantum States of Confined Carriers in Very Thin $Al_xGa_{1-x}As$-GaAs-$Al_xGa_{1-x}As$ Heterostructures. *Phys. Rev. Lett.* **1974**, *33*, 827–830.
54. Negoita, V.; Snoke, D. W.; Eberl, K. Harmonic-Potential Traps for Indirect Excitons in Coupled Quantum Wells. *Phys. Rev. B: Condens. Matter Mater. Phys.* **1999**, *60*, 2661–2669.
55. Ciuti, C.; Schwendimann, P.; Quattropani, A. Theory of Polariton Parametric Interactions in Semiconductor Microcavities. *Semicond. Sci. Technol.* **2003**, *18*, S279–S293.
56. Zinov'ev, N. N.; Ivanov, L. P.; Leng, I. G.; Pavlov, S. T.; Prokaznikov, A. V.; Yaroshetskii, I. D. Exciton Diffusion and the Mechanism of Exciton Momentum Scattering in Semiconductors. *Sov. Phys. JETP* **1983**, *57*, 1254–1262.
57. Takagahara, T. *Quantum Coherence, Correlation and Decoherence in Semiconductor Nanostructures*; Academic Press: London, 2003.
58. Basu, P. K.; Ray, P. Calculation of the Mobility of Two-Dimensional Excitons in a GaAs/$Al_xGa_{1-x}As$ Quantum Well. *Phys. Rev. B: Condens. Matter Mater. Phys.* **1991**, *44*, 1844–1849.